Dalton Transactions

Accepted Manuscript

ROYAL SOCIETY OF CHEMISTRY

www.rsc.org/dalton

Assembly of Various Degrees of Interpenetration Co-MOFs Based on Mononuclear or Dinuclear Cluster Units: Magnetic Properties and Gas Adsoption

Meng-Xi Zheng, Xiang-Jing Gao, Chuan-Lei Zhang, Ling Qin and He-Gen Zheng*

Three new Co-based MOFs with a nanosized tetradentate pyridine ligand, N,N,N',N'-tetrakis(4-(4-pyridine)-phenyl) biphenyl-4,4'-diamine (TPPBDA) and carboxylate co-ligands, $[Co(TPPBDA)(NO_3)_2]_n \cdot 2H_2O$ (**1**), $[Co_2(TPPBDA)(bpdc)_2(H_2O)]_n \cdot 2DMA$ (**2**) and $[Co(TPPBDA)_{0.5}(hfipbb)(H_2O)]_n \cdot 3.5H_2O$ (**3**) (H_2bpdc = biphenyldicarboxylic acid, $H_2hfipbb$ = 4,4'-(hexafluoroisopropylidene)bis-(benzoic acid), DMA = N,N-dimethylacetamide) have been synthesized under hydrothermal conditions. For complex **1**, a large cavity causes 4-fold interpenetration of the network, which can be classified as type IIIa mode of interpenetration. Complex **2** reveals a non-interpenetrating three-dimensional (3D) framework based on $[Co_2(\mu_2\text{-}H_2O)(CO_2)_2]$ unit. Complex **3** is also a 2-fold interpenetrating 3D net based on $[Co_2(CO_2)_2]$ cluster. These mononuclear or dinuclear cluster units are interconnected by TPPBDA and carboxylate co-ligands, resulting in interesting structural diversities and various degrees of interpenetration.

Introduction

Over the past decade, considerable efforts have been made toward the construction and investigation of metal-organic frameworks (MOFs), not only because of their exceptional coordination properties and structural diversity but also because of their

State Key Laboratory of Coordination Chemistry, School of Chemistry and Chemical Engineering, Collaborative Innovation Center of Advanced Microstructures, Nanjing University, Nanjing 210093, P.R. China. E-mail: zhenghg@nju.edu.cn; Fax: 86-25-83314502.

† Electronic supplementary information (ESI) available: PXRD, UV-vis, the selected bond lengths and angles. CCDC: 1040560-1040562 for 1- **3**. For ESI and crystallographic data in CIF or other electronic format see DOI: 10.1039/

intriguing potential applications[1]. The interests in crystalline solids with designed structures and predictable properties continue to motivate research in MOFs in chemistry and material science today[2]. It is noteworthy that utilizing infinite rod-shaped or other secondary building units (SBUs) can reduce the interpenetration, which provides MOFs with permanent porosity and rigid architectures[3]. Although interpenetration in porous MOFs may greatly reduce the volume of pores, it is beneficial to maintain the host frameworks[4]. Thus, the influencing factors on the degree of interpenetration are a large concern for synthetic chemists. To the best of our knowledge, many other cases have been reported about the influencing factors on the interpenetration[5]. Nevertheless, the exploration of the degree of interpenetration controlled by adjusting the SBUs has not exploited well.

Recently, we reported a neutral tetradentate nanosized ligand, N,N,N',N'-tetrakis (4-(4-pyridine)-phenyl) biphenyl-4,4'-diamine (TPPBDA) (Scheme 1).[6] By introduction of different co-ligands, a remarkable range of materials containing various architectures have been prepared. Compared to the reported structures, the nanosized ligand may induce the interpenetration. As continuous exploitation on the study of Co(II)-based MOFs with TPPBDA, three new Co(II)-MOFs, $[Co(TPPBDA)(NO_3)_2]_n \cdot 2H_2O$ (**1**), $[Co_2(TPPBDA)(bpdc)_2\ (H_2O)]_n \cdot 2DMA$ (**2**) and $[Co(TPPBDA)_{0.5}(hfipbb)(H_2O)]_n \cdot 3.5H_2O$ (**3**), have been successfully obtained, in which Co^{2+} cations act as the mononuclear or dinuclear SBUs. These mononuclear or dinuclear units are interconnected by TPPBDA and carboxylate co-ligands, resulting in interesting structural diversities and various degrees of interpenetration.

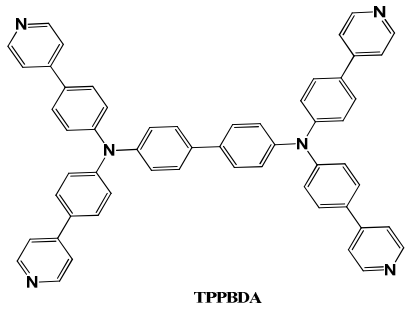

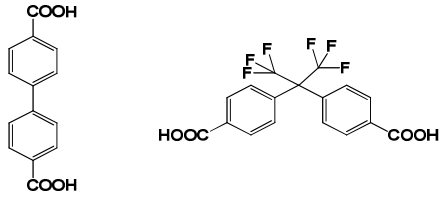

Scheme 1. Neutral tetradentate N-containing ligand and carboxylate co-ligands.

Experimental

Materials and instrumentation

All reagents were of analytical grade and used without further purification. The IR absorption spectra of the complexes were recorded in the range of 400 - 4000 cm^{-1} by means of a Nicolet (Impact 410) spectrometer with KBr pellets. C, H and N elemental analyses were carried out with a Perkin Elmer 240C elemental analyzer. Powder X-ray diffraction (PXRD) measurements were performed on a Bruker D8 Advance X-ray diffractometer using Cu-Kα radiation (1.5418 Å), and the X-ray tube was operated at 40 kV and 40 mA. Temperature dependent magnetic susceptibility data for polycrystalline complex **2** were obtained on a MPMS XL-7 SQUID magnetometer under an applied field of 2000 Oe over the temperature range of 1.8-300 K. The gas sorption isotherms for complex **2** were measured by Micromeritics ASAP 2020 M+C surface area analyzer.

Syntheses of the complexes 1-3: A mixture of H_2O/DMA/CH_3CN containing the TPPBDA (79.6 mg, 0.1 mmol), $Co(NO_3)_2 \cdot 6H_2O$ (58.2 mg, 0.2 mmol) or/and carboxylate co-ligands (0.1 mmol) was mixed in a Teflon vessel within the autoclave.

The vessel was heated at 85 °C for 72 h and then cooled to room temperature. The large amounts of red crystals were obtained. Yields of the reaction were ca. 20%, 70%, 10% based on TPPBDA ligand, respectively. Elemental analysis calcd. for $C_{56}H_{40}CoN_8O_6(H_2O)_2$ (**1**): C, 66.21%; H, 4.37%; N, 11.03%, Found: C, 66.18%; H, 4.35%; N, 11.06%. IR(KBr, cm^{-1}): 3403(s), 3038(w), 1595(s), 1484(s), 1398(m), 1310(m), 1288(s), 1224(m), 1171(m), 1100(m), 1027(w), 998(m), 817(s), 748(m), 702(m), 563(w), 510(m). For $C_{84}H_{58}Co_2N_6O_9(C_4H_9NO)_2$ (**2**): C, 69.60%; H, 4.82%; N, 7.06%. Found: C, 69.56%; H, 4.81%; N, 7.07%. IR(KBr, cm^{-1}): 3399(s), 3031(w), 1595(s), 1517(s), 1486(s), 1388(m), 1321(s), 1291(m), 1175(m), 1086(m), 1039(w), 1006(w), 852(s), 813(s), 770(m), 671(m), 561(m), 522(w), 435(w). For $C_{45}H_{30}CoF_6N_3O_5(H_2O)_{3.5}$ (**3**): C, 58.20%; H, 4.02%; N, 4.52%. Found: C, 58.36%; H, 4.45%; N, 4.67%. IR(KBr, cm^{-1}): 3380(s), 3012(w), 1605(s), 1546(s), 1457(s), 1362(m), 1329(s), 1284(m), 1163(m), 1064(m), 1025(w), 819(s), 751(m), 545(w).

X-ray crystallography

Crystallographic data of **1-3** were collected on a Bruker Apex Smart CCD diffractometer with graphite-monochromated Mo-K_α radiation (λ = 0.71073 Å) at 293 K using the ω-scan technique. The intensity data were integrated by using the SAINT program. An empirical absorption correction was applied using the SADABS program.[7] The structures were solved by direct methods and refined anisotropically using full-matrix least-squares procedures based on F^2 values with the SHELXTL-97 package of crystallographic software.[8] The hydrogen atoms were generated geometrically. Crystallographic data of complexes **1-3** are presented in Table 1, the selected bond lengths and angles are given in Tables S1-S3.

Results and discussion

Description of structures for 1-3

Crystal structure of $[Co(TPPBDA)(NO_3)_2]_n \cdot 2H_2O$ (1). The crystal structure determination reveals that complex **1** crystallizes in orthorhombic crystal system of

Pbcm. In the asymmetric unit, it contains half of one Co(II) cation, half of one TPPBDA ligand, and two halves of NO_3^- anions, and two squeezed lattice water. The Co (II) ion is six-coordinated by four N atoms from four TPPBDA ligands and two NO_3^- anions (Fig. 1a). The tetradentate TPPBDA ligands bridge the Co (II) ions into a 3D network (Fig. 1b). The size of this net is 17.86×17.90Å^2 along the *a* axis. We can consider the Co (II) and the TPPBDA ligands as square-planar and tetrahedral four-connected nodes, respectively, thus giving a short vertex symbol $4^2.8^4$, which is that of the pts topology,[9] as shown in Fig. 1c. It is worth noting that there are 3D channels running along the *a*-, *b*-, and *c*-axes in the structure of **1**. The framework **1** occupies 58% of the total crystal volume; the remaining space is occupied by the solvent molecules. Such a large cavity causes 4-fold interpenetration of the networks, which can be best described as two sets of a normal 2-fold net that is a [2 + 2] mode of interpenetration (Fig. 1d). According to Blatovs' classification which is mainly based on the symmetric relationships between the interpenetrating nets,[10] the interpenetration of **1** can be classified as type IIIa, Z = 4[2*2] (Zt = 2; Zn = 2).

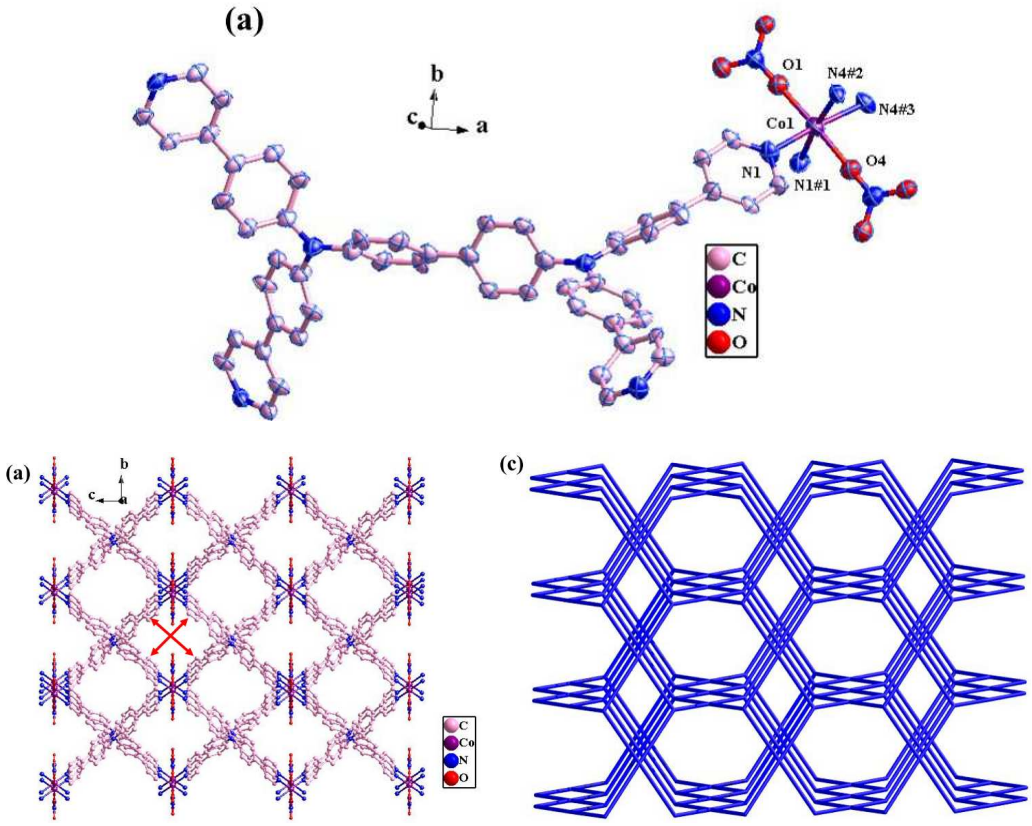

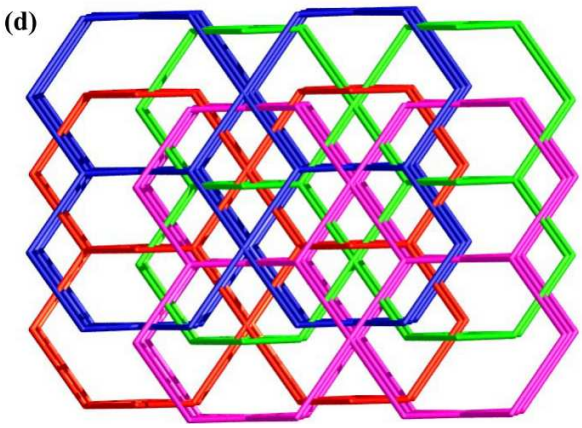

Fig. 1 (a) ORTEP drawing of **1** with 30% ellipsoid probability (hydrogen atoms are omitted for clarity), symmetry codes: #1 = *x*, *y*, 1.5-*z*; #2 = 1+*x*, 1 + *y*, *z*; #3 = 1+ *x*, 1 + *y*, 1.5-*z*. (b) A perspective of 3D framework **1** along the *a* axis. (c) A view of pts topology. (d) Schematic representation of 4-fold interpenetration.

Crystal structure of $[Co_2(TPPBDA)(bpdc)_2(H_2O)]_n$•2DMA (2).

Complex **2** crystallizes in a monoclinic space group *C*2/*c* and features a neutral three-dimensional porous framework. The framework of **2** consists of dinuclear $[Co_2(\mu_2\text{-}H_2O)(CO_2)_2]$ units where each Co center has CoO_4N_2 octahedral coordination geometry and the Co···Co distance is 3.664(4) Å (Fig. 2a). Each $[Co_2(\mu_2\text{-}H_2O)(CO_2)_2]$ unit is doubly bridged by two carboxylate groups and one water molecule, which is further coordinated by four pyridine N atoms and two carboxylate O atoms from two different $bpdc^{2-}$ ligands. The Co-O bond lengths are in the range 2.0508(10)- 2.1629(6) Å, and the Co-N bond lengths are 2.1441(11) and 2.1975(15) Å, which are comparable to those reported in the literature[11]. The TPPBDA and $bpdc^{2-}$ links $[Co_2(\mu_2\text{-}H_2O)(CO_2)_2]$ units to form a 3D structure (Fig. 2b). To reduce multidimensional structures to simple nodes and connection nets, these $[Co_2(\mu_2\text{-}H_2O)(CO_2)_2]$ units, acting as 6-connected nodes, are inter-linked by the 4-connected TPPBDA ligands and H_2bpdc linkers into a 3D open framework with 4,6-connected topology (Fig. 2c). According to a calculation performed using PLATON, compound **2** contains a solvent accessible void space of 26% of the total

crystal volume.

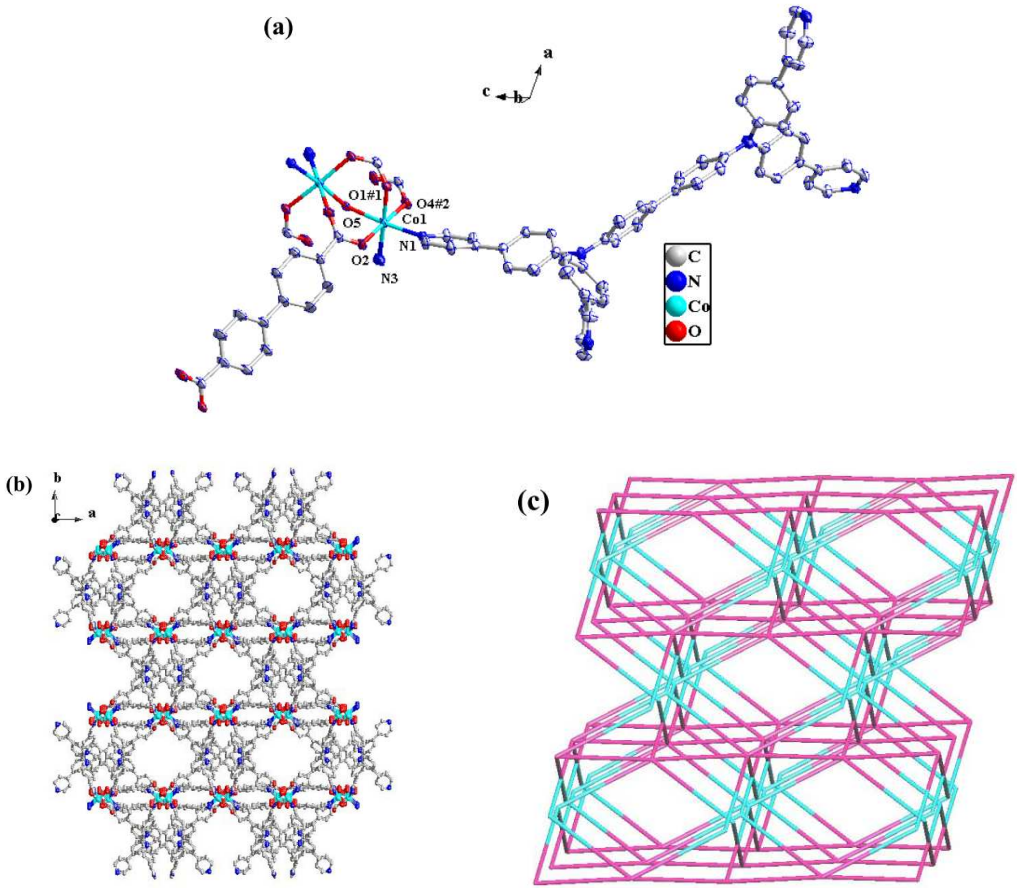

Fig. 2 (a) ORTEP drawing of **2** with 30% ellipsoid probability (hydrogen atoms and lattice water molecules are omitted for clarity), symmetry codes: #1 = 1 - *x*, *y*, 1.5-*z*; #2 = 0.5 + *x*, 0.5 - *y*, -0.5 + *z*. (b) A perspective of 3D framework **2**. (c) Schematic representation of topology.

Crystal structure of $[Co(TPPBDA)_{0.5}(hfipbb)(H_2O)]_n \cdot 3.5H_2O$ (3).

Complex **3** crystallizes in the monoclinic crystal system with one Co cation, half of TPPBDA, one $hfipbb^{2-}$ ligand, as well as one coordinated water molecule, and three and a half molecules of water in the asymmetric unit. Each Co(II) unit has an octahedral coordination geometry (Fig. 3a). The $hfipbb^{2-}$ ligand takes bidentate and monodentate coordination modes, two Co(II) ions are bridged by two carboxylate O atoms forming a four-membered square-shaped $[Cd_2(CO_2)_2]$ unit. The $hfipbb^{2-}$ anions connect to the $[Cd_2(CO_2)_2]$ units to form 1D chains. Then the chains are linked by the

neutral tetradentate ligand to generate a 3D net (Fig. 3b).

Complex **3** is a three-dimensinal net composed of meso-helical chains, which are labeled as L and R chains (Fig. 3c). Similarly, the two symmetrically related helices coexist in the centrosymmetric solid, in which they show left-handed and right-handed enantiomorphs, respectively. However, the L and R type single meso-helical chains are arranged alternatively, which indicates the achirality feature, further confirmed by the achiral space group *C*2/*m*. The central axis is a 2-fold screw axis.

To better insight into the nature of the intricate framework, topological approach can be applied. As discussed above, $[Co_2(CO_2)_2]$ cluster units are defined as 6-connected nodes. Likewise, TPPBDA ligands linking with four $[Co_2(CO_2)_2]$ cluster units can act as 4-connected nodes. On the basis of the simplification principle, the resulting structure is a (4,6)-connected net with point symbol $\{4^6\}\{4^2.6^8.8^5\}$ (Fig 3d). Compound **3** contains a solvent accessible void space of 42.5% of the total crystal volume. In order to minimize the big void cavities and stabilize the framework, the potential voids formed by a single 3D network show incorporation with one other identical network, thus giving a 2-fold interpenetrating network (Fig. 3e).

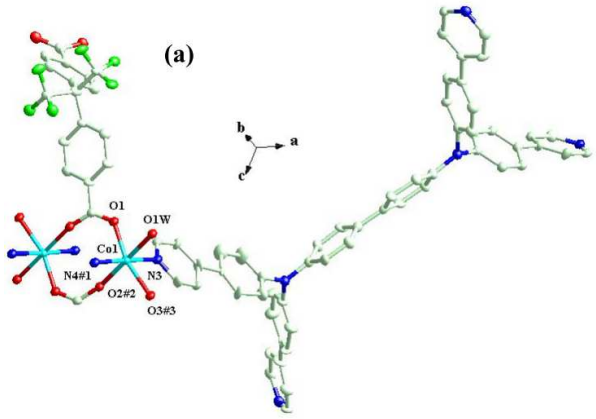

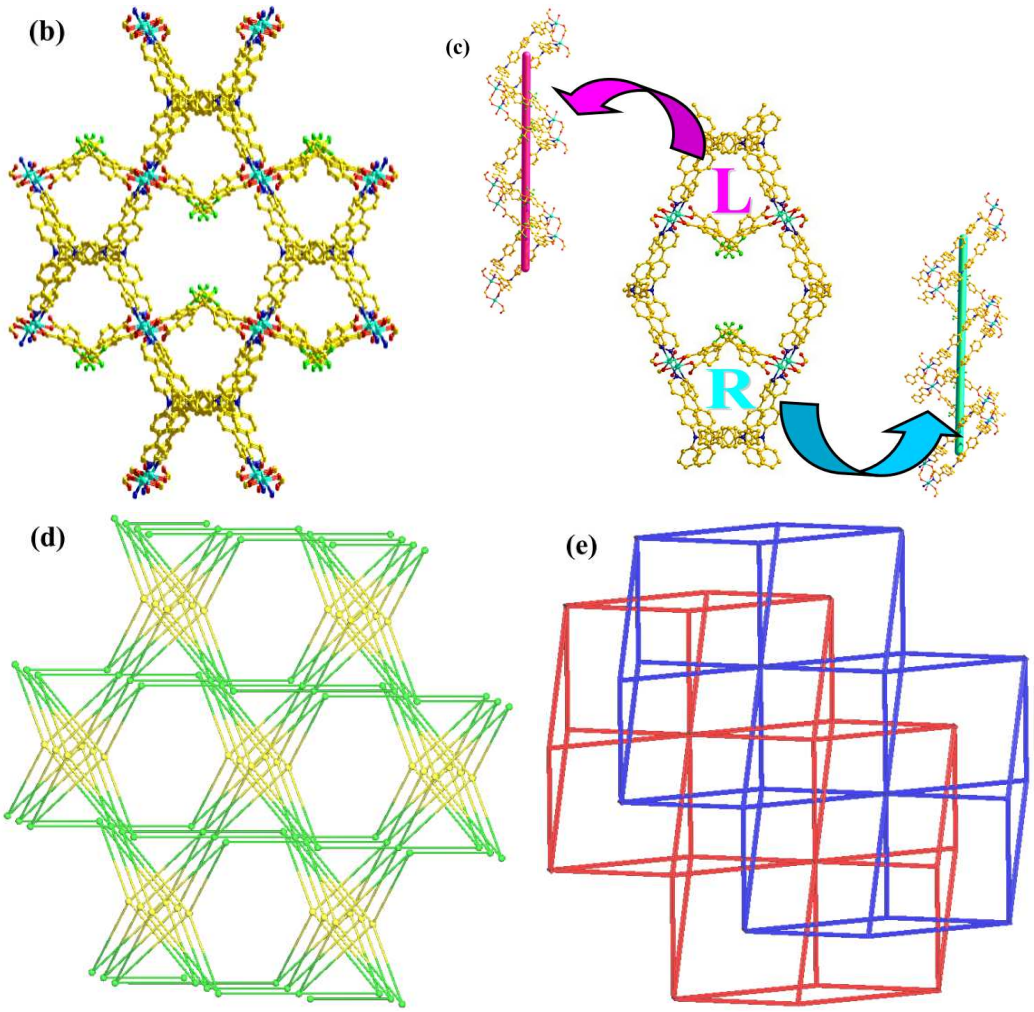

Fig. 3 (a) ORTEP drawing of **3** with 30% ellipsoid probability (hydrogen atoms are omitted for clarity), symmetry codes: #1 = -0.5 + *x*, 0.5 + *y*, 1 + *z*; #2 = 1.5 - *x*, 0.5 - *y*, 2 - *z*; #3 = 0.5 + *x*, 0.5 - *y*, 1 + *z*. (b) A perspective of 3D framework **3**. (c) View of meso-helical chains (marked by L and R) in net **3**. (d) and (e) Schematic representation of topology and 2-fold interpenetration.

Gas uptake properties of 2

To check the permanent porosities, N_2 sorption isotherms at 77 K were measured for the desolvated samples obtained by soaking **2** in acetone, and then vacuum-drying at 90℃ overnight. As shown in Fig. 4 (left), **2** displays typical type-I adsorption isotherms. **2** adsorbs 157 cm^3g^{-1} of N_2 at 77 K, and the Brunauer-Emmett-Teller (BET)

and Langmuir surface areas are 468m^2g^{-1} and 702m^2g^{-1}, respectively. Low-pressure CH_4 uptakes of desolvated samples of **2** were also determined using volumetric gas adsorption measurements. The adsorption isotherms were fully reversible, and exhibit 14 cm^3g^{-1} CH_4 uptake under the conditions of 273 K and 850 mmHg. However, the adsorption amount of CO_2 is 61cm^3g^{-1} under the same conditions (Fig. 4, right). At room temperature and 850 mmHg, the CO_2 uptake of **2** is 29 cm^3g^{-1} (Fig. 5, left). The isosteric heats of adsorption (Q_{st}) were calculated from the CO_2 adsorption isotherms by using the Clausius-Clapeyron equation (Supporting Information), which is similar to values for some other MOF materials (Fig. 5, right). [12] The result shows that CO_2 and CH_4 isotherms at 273 K reach the maximums of 61cm^3g^{-1} and 14cm^3g^{-1}, respectively. When the pressure is increased, the CO_2 adsorption capacity greatly exceeded that of CH_4. The results show that **2** has a potential application in gas separation processes of CH_4/CO_2.

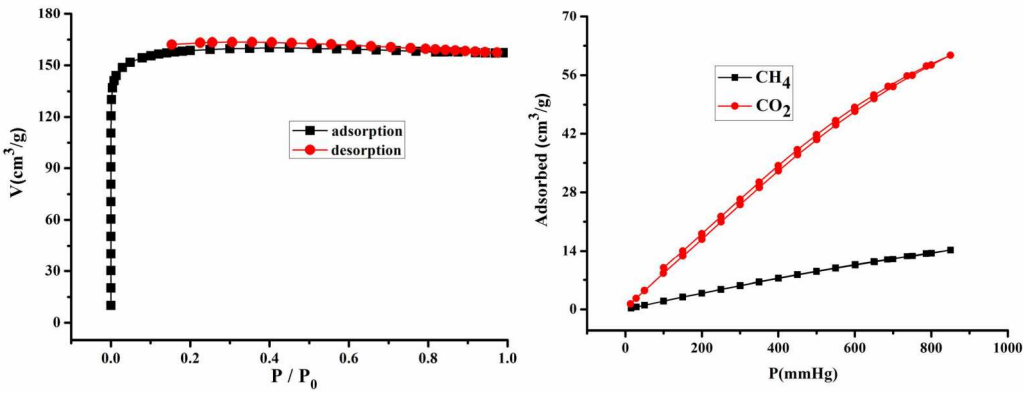

Fig. 4 Left: Nitrogen isotherms measured at 77 K (black and red represent adsorption and desorption branches, respectively). Right: CO_2 and CH_4 sorption isotherms measured at 273 K.

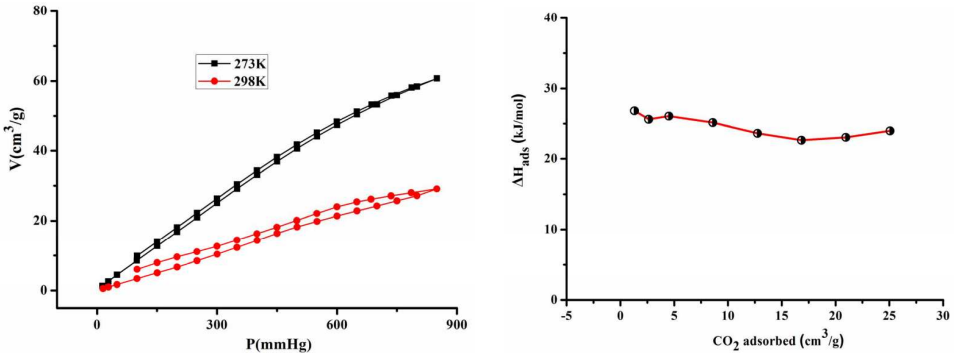

Fig. 5 Left: CO_2 gas adsorption isotherms at 273 K and 298K. Right: The isosteric heats of adsorption were calculated from the CO_2 adsorption isotherms by using the Clausius-Clapeyron equation in complex **2**.

Magnetic properties of 2

Temperature dependent magnetic susceptibilities of **2** were investigated in the temperature range of 1.8-300 K. The temperature dependence of magnetic susceptibility of **2** in the forms of $\chi_M T$ and χ_M versus T is displayed in Fig 6, the experimental $\chi_M T$ value equal to 4.81 $cm^3\ K\ mol^{-1}$ at 300 K is greater than the expected value of 3.75 $cm^3\ K\ mol^{-1}$ for two isolated high-spin Co(II) ions (g = 2 and S = 3/2) per formula because of the prominent orbital contribution contribution arising from the $4T_{1g}$ ground state of Co(II). Upon cooling, $\chi_M T$ continuously decreases and reaches 0.73 $cm^3\ K\ mol^{-1}$ at 1.8K. The magnetic susceptibility data were fitted assuming that the carboxylate and oxygen bridges of the Co(II) ions form an isolated spin dimer system. The intermolecular magnetic coupling constant *zj*' was taken into account, the magnetic susceptibility from 7-300K was fitted with equation (1), which is deduced from the spin Hamiltonian, $H = -2JS_1S_2$: [13]

$$\hat{H} = -2J\hat{S}_1\hat{S}_2 = -J(\hat{S}_T^2 - \sum_{i=1}^{2}\hat{S}^2)$$

$$E(S_T) = -JS_T(S_T+1)$$

$$S_T = 0, 1, 2, 3$$

$$E(S_T) = 0, -2J, -6J, -12J$$

$$\chi_{\mathrm{M}} = \frac{Ng^2\beta^2}{3kT} \times \frac{84e^{12J/kT} + 30e^{6J/kT} + 6e^{2J/kT}}{7e^{12J/kT} + 5e^{6J/kT} + 3e^{2J/kT} + 1} \quad (1)$$
$$= \frac{2Ng^2\beta^2}{kT} \times \frac{14e^{12J/kT} + 5e^{6J/kT} + e^{2J/kT}}{7e^{12J/kT} + 5e^{6J/kT} + 3e^{2J/kT} + 1}$$

An excellent fit was obtained with J = -6.70 cm^{-1}, zj' = -1.07cm^{-1} and g = 2.17 with an agreement factor $R = 3.7 \times 10^{-7}$. This result also indicates antiferromagnetic coupling between two Co^{II} centers through two carboxylate bridges and two oxygen bridges.

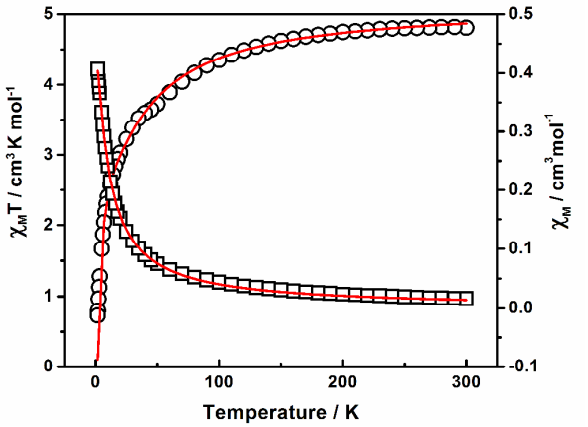

Fig. 6 Temperature dependence of χ_M and $\chi_M T$ for **2** (open circles and red line represent experimental data and fits).

Conclusion

In summary, three Co-MOFs have been successfully obtained, in which Co^{2+} cations act as the mononuclear or dinuclear SBUs.[14] The interpenetration forms were well tuned by Co^{2+} cations as different mononuclear or dinuclear SBUs: a large cavity causes 4-fold interpenetration for mononuclear Co^{2+} cations in complex **1**; complex **2** shows a non-interpenetrating 3D framework based on $[Co_2(\mu_2\text{-}H_2O)(CO_2)_2]$ unit; whereas complex **3** reveals a 2-fold interpenetrating 3D framework with dinuclear $[Co_2(CO_2)_2]$ unit. The magneto-chemical analysis of complex **2** indicates that there are dominant antiferromagnetic interactions between Co^{2+} ions in these systems. In addition, complex **2** exhibits microporous sorption for N_2, CO_2 and CH_4.

Acknowledgments

This work was supported by grants from the National Undergraduate Innovation Training Program (201410284036), the National Natural Science Foundation of China (Nos. 21371092; 91022011), National Basic Research Program of China (2010CB923303).

References

[1] (a) J. E. Clements, J. R. Price, S. M. Neville and C. J. Kepert, *Angew. Chem. Int. Ed*., 2014, **53**, 10164; (b) W. Cho, H. J. Lee, G. Choi, S. Choi and M. Oh, *J. Am. Chem. Soc*., 2014, **136**, 12201; (c) W. Kosaka, K. Yamagishi, J. Zhang and H. Miyasaka, *J. Am. Chem. Soc*., 2014, **136**, 12304; (d) D. E. Williams, J. A. Rietman, J. M. Maier, R. Tan, A. B. Greytak, M. D. Smith, J. A. Krause and N. B. Shustova, *J. Am. Chem. Soc*., 2014, **136**, 11886; (e) C. Wang, J. L. Wang and W. B. Lin, *J. Am. Chem. Soc*. 2012, **134**, 19895; (f) C. Wang and W. B. Lin, *J. Am. Chem. Soc.* 2011, **133**, 4232.

[2] (a) Z. Xu, W. Meng, H. Li, H. Hou and Y. Fan, *Inorg. Chem*., 2014, **53**, 3260; (b) J. Qin, Y. Jia, H. Li, B, Zhao, D. Wu, S. Zang, H. Hou and Y. Fan, Inorg. Chem., 2014, **53**, 685; (c) Y. Y. Zhang, X. Y. Shen, L. H. Weng and G. X. Jin, *J. Am. Chem. Soc*., 2014, **136**, 15521; (d) S. L. Huang, Y. J. Lin, Z. H. Li, G. X. Jin, *Angew. Chem. Int. Ed*., 2014, **53**, 11218; (e) J. T. Shi, K. F. Yue, B. Liu, C. S. Zhou, Y. L. Liu, Z. G. Fanga and Y. Y. Wang, *CrystEngComm*, 2014, **16**, 3097; (f) B. Wang, Z. P. Zang, H. H. Wang, W. Dou, X. L. Tang, W. S. Liu, Y. L. Shao, J. X. Ma, Y. Z. Li and J. Zhou, *Angew. Chem., Int. Ed*., 2013, **52**, 3756; (g) Y. Han, H. Xu, Y. Y. Liu, H. J. Li, H. W. Hou, Y. T. Fan and S. R. Batten, *Chem. Eur. J*., 2012, **18**, 13954; (h) H. Zhang, Y. Lu, Z. M. Zhang, H. Fu, Y. G. Li, D. Volkmer, D. Denysenko and E. B. Wang, *Chem. Commun*., 2012, **48**, 7295.

[3] (a) Y. Bu, F. Jiang, K. Zhou, Y. Gai and M. Hong, *CrystEngComm*, 2014, **16**, 1249; (b) N. L. Rosi, J. Kim, M. Eddaoudi, B. Chen, M. O'Keeffe and O. M. Yaghi, *J. Am. Chem. Soc*. 2005, **127**, 1504.

[4] L. Ma and W. Lin, *Angew. Chem. Int. Ed*., 2009, **48**, 3637.

[5] (a) J. Duan, J. Bai, B. Zheng, Y. Li and W. Ren, *Chem. Commun*., 2011, **47**, 2556; (b) J. J. Zhang, L. Wojtas, R. W. Larsen, M. Eddaoudiand M. J. Zaworotko, *J. Am. Chem. Soc.*, 2009, **131**, 17040; (c) Y. Yamauchi, M. Yoshizawa and M. Fujita, *J. Am. Chem. Soc*., 2008, **130**, 5832; (d) T. K. Maji, R. Matsuda and S. Kitagawa, *Nat. Mater*., 2007, **6**, 142; (e) A. Galet, V. Niel, M. C. Munoz and J. Real, *J. Am. Chem. Soc*., 2003, **125**, 14224; (f) T. M. Reineke, M. Eddaoudi, D. Moler, M. O′Keeffe and O. M. Yaghi, *J. Am. Chem. Soc*., 2000, **122**, 4843.

[6] (a) L. Qin, H. L. Jia, Z. J. Guo and H. G. Zheng, *Cryst. Growth Des*., 2014, **14** 6607. (b) L. Qin, Z. M. Ju, Z. J. Wang, F. D. Meng, H. G. Zheng and J. X. Chen, *Cryst. Growth Des*., 2014, **14**, 2742; (c) L. Qin, M. D. Zhang, Q. X. Yang, Y. Z. Li and H. G. Zheng, *Cryst. Growth Des*., 2013, **13**, 5045.

[7] G. M. Sheldrick, *SADABS*, *Program for Bruker Area Detector Absorption Correction,* University of Göttingen, Göttingen, Germany, 1997.

[8] Bruker 2000, SMART (Version 5.0), SAINT-plus (Version 6), SHELXTL (Version 6.1), and SADABS (Version 2.03); Bruker AXS Inc.: Madison, WI.

[9] V. A. Blatov, A. P. Shevchenko and V. N. Serezhkin, *J. Appl. Crystallogr.*, 2000, **33**, 1193.

[10] (a) V. A. Blatov, L. Carlucci, G. Ciani and D. M. Proserpio, *CrystEngComm*, 2004, **6**, 378; (b) I. A. Baburin, V. A. Blatov, L. Carlucci, G. Ciani and D. M. Proserpio, *J. Solid State Chem.*, 2005, **178**, 2452.

[11] (a) Y. Yan, C. D. Wu, X. He, Y. Q. Sun and C. Z. Lu, *Cryst. Growth Des*., 2005, **5**, 821; (b) D. R. Xiao, E. B. Wang, H. Y. An, Y. G. Li, Z. M. Su and C. Y. Sun, *Chem. Eur. J.*, 2006, **12**, 6528; (c) S. Q. Zang, Y. Su, Y. Z. Li, H. Z. Zhu and Q. J. Meng, *Inorg. Chem.*, 2006, **45**, 2972.

[12] (a) P. L. Llewellyn, S. Bourrelly, C. Serre, A. Vimont, M. Daturi, L. Hamon, G. D. Weireld, J. S. Chang, D. Y. Hong, Y. K. Hwang, S. H. Jhung and G. Férey, *Langmuir* 2008, **24**, 7245; (b) T. Loiseau, L. Lecroq, C. Volkringer, J. Marrot, G. Férey, M. Haouas, F. Taulelle, S. Bourrelly, P. L. Llewellyn and M. Latroche, *J. Am. Chem. Soc.*, 2006, **128**, 10223; (c) Q. M. Wang, D. Shen, M. Bülow, M. L.

Lau, S. Deng, F. R. Fitch, N. O. Lemcoff and J. Semanscin, *Microporous Mesoporous Mater.,* 2002, **55**, 217.

[13] O. Kahn, Molecular Magnetism; VCH Publishers: New York, 1993.

[14] (a) L. Qin, J. S. Hu, M. D. Zhang, Z. J. Guo and H. G. Zheng, *Chem. Commun.* **2012**, **48**, 10757. (b) N. L. Rosi, J. Kim, M. Eddaoudi, B. Chen, M. O'Keeffe and O. M. Yaghi, *J. Am. Chem. Soc*. 2005, **127**, 1504. (c) T. M. Reineke, M. Eddaoudi, D. Moler, M. O'Keeffe and O. M. Yaghi, *J. Am. Chem. Soc*. 2000, **122**, 4843.

Table 1 Crystal data and structure refinements parameters of complexes **1**, **2** and **3**

Complex	**1**[a]	**2**[a]	**3**[a]
Empirical formula	$C_{56}H_{40}CoN_8O_6$	$C_{84}H_{58}Co_2N_6O_9$	$C_{45}H_{30}CoF_6N_3O_5$
Formula weight	979.89	1413.22	865.65
Crystal system	Orthorhombic	Monoclinic	Monoclinic
space group	*Pbcm*	*C*2/*c*	*C*2/*m*
a(Å)	20.7677(15)	22.2737(18)	22.8097(18)
b(Å)	11.7553(9)	29.146(2)	36.6950(15)
c(Å)	28.509(2)	13.8719(12)	14.4183(11)
α(°)	90	90	90
β(°)	90	108.451(2)	106.313(2)
γ(°)	90	90	90
Volume ($Å^3$)	6959.9(9)	8542.6(12)	11582.3(14)
Z	4	4	8
D_c,g cm^{-3}	0.935	1.099	0.993
Absorptioncoefficient,mm^1	0.289	0.442	0.351
F(000)	2028	2920	3536
Reflections collected /	36797 / 7005	21281 / 7552	42053 / 14579
unique	[R(int) = 0.0129]	[R(int) = 0.0364]	[R(int) = 0.0106]
Data/restraints/paramers	7005 / 0 / 337	7552 / 378 / 511	14579 / 0 / 676
Goodness-of-fit on F^2	1.034	1.018	1.003
Final R indices [I>2σ(I)]	R1[b] = 0.0484,	R1[b] = 0.0520,	R1[b] = 0.0392,
	wR2[c] =0.1235	wR2[c] = 0.1448	wR2[c] = 0.1383
Largest diff.and hole e.$Å^{-3}$	0.240 and -0.334	0.544 and -0.462	0.291 and -0.268

[a] The residual electron densities were flattened by using the SQUEEZE option of PLATON.

[b] $R1 = \Sigma||F_o|-|F_c||/|\Sigma|F_o|$.

[c] $wR2 = \{\Sigma[w(F_o^2-F_c^2)^2]/\Sigma[w(F_o^2)^2]\}^{1/2}$; where $w = 1/[\sigma^2(F_o^2)+(aP)^2+bP]$, $P = (F_o^2+2F_c^2)/3$.

Assembly of Various Degrees of Interpenetration Co-MOFs Based on Mononuclear or Dinuclear Cluster Units: Magnetic Properties and Gas Adsoption

Meng-Xi Zheng, Xiang-Jing Gao, Chuan-Lei Zhang, Ling Qin and He-Gen Zheng*

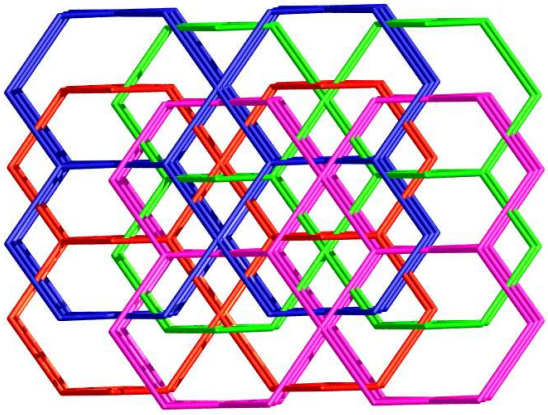

The mononuclear or dinuclear Co cluster units are interconnected by mixed ligands, resulting in interesting structural diversity and various degrees of interpenetration.